(Received 5 June 2024, Accepted 15 July 2024, Scheduled 20 July 2024)

Square-Coupled Topological Filter with an Ideal Rectangular Coefficient Facilitated by Dual-Cavity Single-Mode and Single-Cavity Dual-Mode SIW Resonators

Xiaohei Yan and Wenjing Mu*

School of Mathematics, Physics, and Electronic Information Engineering
Guangxi Minzu Normal University, Chongzuo 532200, China

ABSTRACT: In order to achieve miniaturization and high performance in microwave filters, this paper proposes two double-layer bandpass filters with different structures, both equivalent to square-coupled topologies. These filters employ dual-cavity single-mode and single-cavity dual-mode substrate-integrated waveguide resonators. In this configuration, the upper layer comprises two single-mode resonators connected to the input and output feed lines, while the lower layer contains dual-mode resonators coupled to the upper layer's single-mode resonators through two slots on the middle metal layer. A comprehensive analysis is conducted on the impact of primary parameters on filter characteristics and transmission zero positions. The second filter is fabricated and tested, yielding results consistent with simulation outcomes. The center frequency of the filter is 4.77 GHz, with a 3 dB bandwidth of 0.16 GHz (relative bandwidth: 3.35%). Additionally, its rectangularity coefficient at 10 dB approximately equals one, an ideal value for practical applications.

1. INTRODUCTION

Substrate-integrated waveguide (SIW) is highly favored in modern communication systems' radio frequency (RF) front-end circuits due to its planar design, lightweight nature, high Q factor, and seamless integration with other microwave circuits. Consequently, the research on designing and developing miniaturized yet high-performance microwave filters using substrate-integrated waveguides has gained significant attention [1–6].

Filters designed using SIW technology can be achieved by utilizing single-mode, dual-mode, and multimode resonators, as well as combined resonator structures. In the design of filters employing single-mode SIW resonators, the introduction of cross-coupling paths with negative coupling coefficients or frequency-varying coupling paths is necessary to enhance passband edge steepness. This is accomplished by generating finite transmission zeros (FTZs) within the stopband. However, implementing negative coupling and frequency-variable coupling with slot-line structures may result in a reduction in the quality factor (Q) of the SIW resonator. To preserve the high Q characteristic of the SIW, higher modes within the SIW resonator, such as TE_{201} mode, can be utilized to generate filter transmission zeros instead. By doing so, equivalent negative coupling paths are provided while avoiding any drawbacks associated with a notch-line structure. This methodology ensures that the requisite filter performance standards are met while fully leveraging the potential of SIW [7–11].

When constructing a filter using a dual-mode SIW resonator, FTZs may be generated by employing two coupling paths and one resonant mode as the equivalent negative coupling path, leading to a passband that is highly selective. The filter designed to utilize a single-cavity dual-mode resonator can be implemented as a two-order filter with two frequency transmission zeros (FTZs). To design more selective and higher-order substrate-integrated waveguide (SIW) filters, [12] and [13] provide a dual-cavity, dual-mode SIW filter design approach that relies on a single-layer structure. This method is capable of realizing two FTZs, but at the cost of a larger size and a less controllable position of FTZs. In contrast, previous research [14] offers a dual-cavity, dual-mode method for designing SIW filters using a double-layer structure. Although this method yields a small size, it suffers from poor controllability of the FTZs' positions. Another approach found in earlier literature [15] involves a dual-cavity single-mode or single-cavity dual-mode SIW filter design using a single-layer structure, which offers better control of the FTZs' position but results in a larger size. In [16, 17], novel planar dual-mode SIW cavity designs are proposed and analyzed with the aim of developing dual-mode filters. This design methodology leads to the formation of FTZs on both sides of the passband, although once again, the filters' size remains significant.

The aforementioned research presents certain challenges, such as excessive size of the filter or the inadequate controllability of FTZs' positions. For microwave filters that require high performance and miniaturization, this study analyzes equivalent coupling topologies of combination filters consisting of single-cavity dual-mode and dual-cavity single-mode resonators. The study proposes two bandpass filter structures, which are equivalent to a square coupling topology. Filter A

* Corresponding author: Wenjing Mu (muwenjing@gxnun.edu.cn).

utilizes two coupling paths and a resonant mode of the single-cavity dual-mode resonator as the equivalent negative coupling path, achieving two FTZs and a highly selective passband. Filter B enhances the rectangular coefficient of the filter by including an inductive coupling window between the two single-mode SIW resonators in the upper layer, creating a direct diagonal coupling path. Finally, filter B underwent processing and testing, and the test results demonstrated consistency with the simulation results, showcasing the feasibility of the dual-layer dual-cavity single-mode and single-cavity dual-mode substrate-integrated waveguide filter structures. The proposed filter structure boasts advantages in miniaturization, ideal rectangular coefficients, and the ability to control transmission zero position.

2. STRUCTURE OF THE FILTER

This design utilizes a substrate-integrated waveguide cavity structure with a double-layer configuration, as illustrated in Figure 1. This structure comprises three metal layers and two dielectric layers, with the dielectric layer composed of RO4350B material having a relative permittivity of 3.66 and a loss tangent of 0.0037. The square-shaped substrate-integrated waveguide cavity contains two triangular single-mode resonance cavities operating in TE_{110} modes in the upper cavity and one double-mode resonance cavity operating in TE_{120} and TE_{210} modes in the lower cavity. To achieve energy coupling between the upper and lower resonant cavities, two slots are etched on the middle metal layer near the edges of the resonant cavities, and their positions are orthogonal. Two metal perturbation holes are placed diagonally on the lower dual-mode resonant cavity to modify the electric field distribution of the TE_{210} mode and to distinguish the resonant frequencies of the TE_{120} and TE_{210} modes. The two filters differ structurally in their upper metal layers. Filter A has two single-mode resonant cavities in the upper layer without a direct diagonal coupling path, while filter B has an added inductive coupling window to form a direct diagonal coupling path. Please refer to Figure 2 for the shape of the metal layers of the filters. After conducting simulations and optimization using the HFSS software, Tables 1 and 2 display the ultimate structural parameters for both filters.

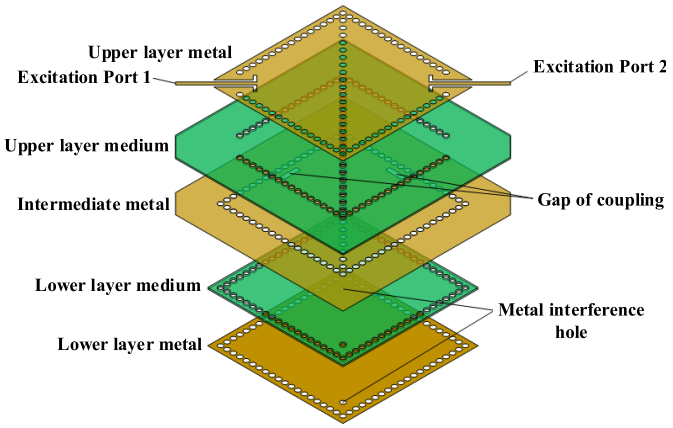

FIGURE 1. Structure of the filter.

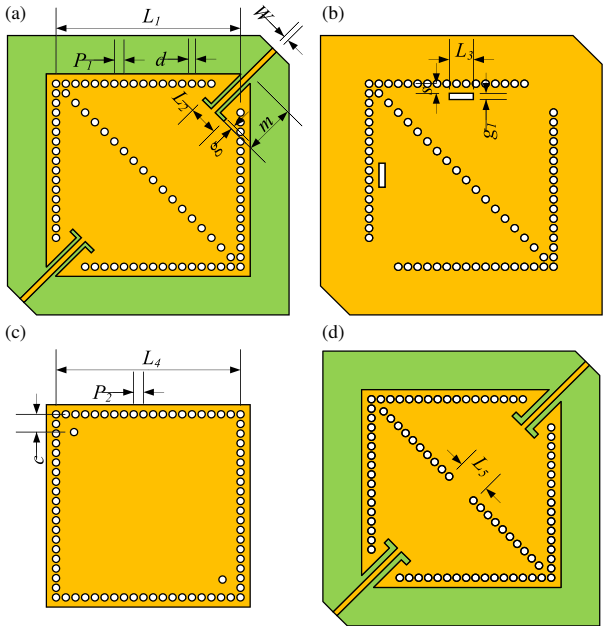

FIGURE 2. Dimensional drawings of the metal layers. (a) Upper metal layer of filter A; (b) Middle metal of filter A; (c) Lower metal layer of filter A; (d) Upper metal layer of filter B.

TABLE 1. Structural parameters of filter A (unit: mm).

$L_1 = 38$	$P_1 = 2$	$d = 0.75$	$W = 1.1$
$m = 22.1$	$g = 0.8$	$L_2 = 6.2$	$L_3 = 5$
$s = 2$	$g_1 = 1.3$	$L_4 = 38$	$P_2 = 2$
$c = 3.7$			

TABLE 2. Structural parameters of filter B (unit: mm).

$L_1 = 37.05$	$P_1 = 1.95$	$d = 0.75$	$W = 1.1$
$m = 22.3$	$g = 1.2$	$L_2 = 6.5$	$L_3 = 5$
$s = 2$	$g_1 = 1.3$	$L_4 = 38$	$P_2 = 2$
$c = 5$	$L_5 = 7$		

3. FILTER DESIGN AND PRINCIPLE ANALYSIS

In this particular design, the upper resonant cavity consists of two triangular single-mode resonant cavities operating in TE_{110} mode. The lower resonant cavity, on the other hand, is a double-mode resonant cavity operating in TE_{120} and TE_{210} modes. The resonant electric field distributions of both cavities are illustrated in Figure 3.

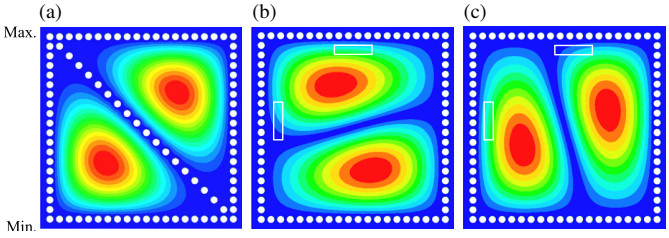

FIGURE 3. Electric field strength distribution in the cavities. (a) TE_{110} mode; (b) TE_{210} mode; (c) TE_{120} mode.

The resonant frequency f_{mn0} of a square substrate-integrated waveguide cavity operating in TE_{mn0} mode can be calculated from the relationship between the cavity dimensions and the mode resonant frequency, which is given by [6]:

$$f_{\mathrm{TE}_{mn0}} = \frac{c_0}{2\sqrt{\varepsilon_r}}\sqrt{\left(\frac{m}{L_{eff}}\right)^2 + \left(\frac{n}{L_{eff}}\right)^2} \tag{1}$$

where ε_r is the dielectric constant of the dielectric substrate; m, n are the numbers of modes along the width and length directions; L_{eff} is the equivalent side length of the SIW cavity, which is defined as follows [6]:

$$L_{eff} = L - \frac{d^2}{0.95P} \tag{2}$$

where L is the center distance between two columns of circular holes in the cavity, d the diameter of the circular holes, and P the centroidal distance between adjacent circular holes. In this design, the filters operate in the 5G n79 band, so the resonant frequency of TE_{120} mode or TE_{210} mode is initially taken to be 4.75 GHz, and the preliminary dimension of the cavity can be calculated according to Eqs. (1) and (2):

$$L \approx 38\,\mathrm{mm} \tag{3}$$

The square cavity can be split into two identical triangular cavities by inserting a row of metal through-holes along the diagonal of the square. Additionally, the resonant frequency of the TE_{110} mode of the triangular cavity corresponds to that of the TE_{120} or TE_{210} mode of the square cavity.

Two slots are engraved on the middle metal layer near the edge of the resonating cavity to achieve energy coupling between the upper and lower cavities. The positions of the two slots are perpendicular. Based on the coupling slot positions shown in Figure 3, it is apparent that the two slots have identical electric field phases in the TE_{210} mode and opposing electric field phases in the TE_{120} mode. Therefore, the coupling of the two coupling slots to the TE_{120} mode can be equated to a negative coupling path.

The coupling topology of filter A is equivalent to the square structure displayed in Figure 4. The corresponding coupling matrix can be represented as follows:

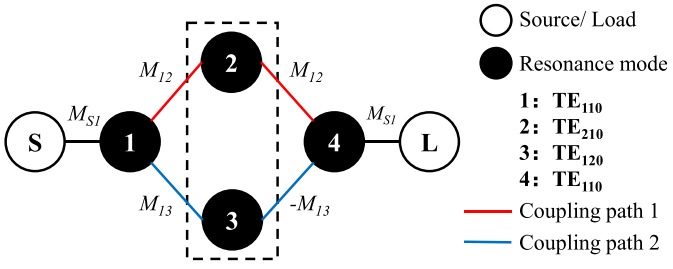

FIGURE 4. Coupling topology of filter A.

$$\begin{bmatrix} 0 & M_{s1} & 0 & 0 & 0 & 0 \\ M_{s1} & 0 & M_{12} & M_{13} & 0 & 0 \\ 0 & M_{12} & 0 & M_{23} & M_{24} & 0 \\ 0 & M_{13} & M_{23} & 0 & -M_{34} & 0 \\ 0 & 0 & M_{24} & -M_{34} & 0 & M_{s1} \\ 0 & 0 & 0 & 0 & M_{s1} & 0 \end{bmatrix} \tag{4}$$

Based on its final S-parameter profile, the filter's coupling matrix can be extracted using the CoupleFil software as

$$\begin{bmatrix} 0 & 0.913 & 0 & 0 & 0 & 0 \\ 0.913 & 0 & 0.541 & 0.588 & 0 & 0 \\ 0 & 0.541 & 0 & 0.077 & 0.541 & 0 \\ 0 & 0.588 & 0.077 & 0 & -0.588 & 0 \\ 0 & 0 & 0.541 & -0.588 & 0 & 0.913 \\ 0 & 0 & 0 & 0 & 0.913 & 0 \end{bmatrix} \tag{5}$$

The source and load are coupled to the upper single-mode resonators 1 and 4, respectively, and both resonators 1 and 4 are coupled to the lower dual-mode resonator in two modes 2 and 3. Two main coupling paths, 1-2-4 and 1-3-4, exist in the filter, and since 1-3-4 is a negative coupling path, FTZs can be realized to improve the selectivity of the filter. The location of the FTZs is mainly affected by the coupling strengths (M_{12} and M_{13}) and the resonance frequencies of the dual-mode resonator.

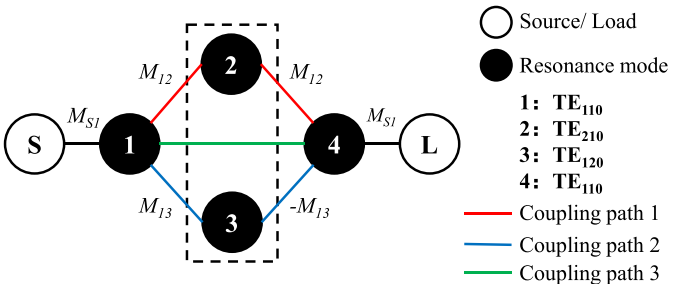

FIGURE 5. Coupling topology of filter B.

The coupling topology for filter B is depicted in Figure 5, and the corresponding coupling matrix is expressed as follows:

$$\begin{bmatrix} 0 & M_{s1} & 0 & 0 & 0 & 0 \\ M_{s1} & 0 & M_{12} & M_{13} & M_{14} & 0 \\ 0 & M_{12} & 0 & M_{23} & M_{24} & 0 \\ 0 & M_{13} & M_{23} & 0 & -M_{34} & 0 \\ 0 & M_{14} & M_{24} & -M_{34} & 0 & M_{s1} \\ 0 & 0 & 0 & 0 & M_{s1} & 0 \end{bmatrix} \tag{6}$$

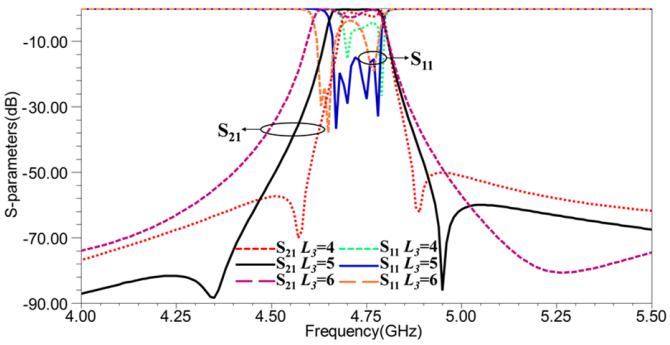

FIGURE 6. S-parameter curves for different values of L_3.

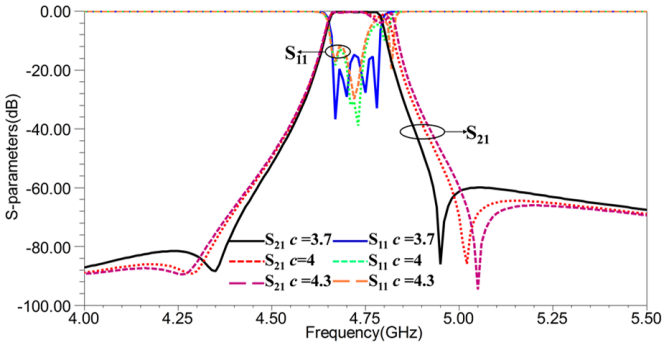

FIGURE 7. S-parameter curves for different values of c.

Based on its final S-parameter profile, the filter's coupling matrix can be extracted using the CoupleFil software as

$$\begin{bmatrix} 0 & 0.897 & 0 & 0 & 0 & 0 \\ 0.897 & 0 & 0.438 & 0.498 & 0.440 & 0 \\ 0 & 0.438 & 0 & 0.053 & 0.438 & 0 \\ 0 & 0.498 & 0.053 & 0 & -0.498 & 0 \\ 0 & 0.440 & 0.438 & -0.498 & 0 & 0.897 \\ 0 & 0 & 0 & 0 & 0.897 & 0 \end{bmatrix} \tag{7}$$

Filter B adds an inductive coupling window between the two single-mode resonant cavities in the upper layer, creating a direct diagonal coupling path 1–4. Obviously, the introduction of the new coupling path inevitably has an effect on the passband of the filter and the position of the FTZs.

In order to achieve the regulation of the passbands and the positions of the FTZs of the filter by modulating the resonant frequency of the lower dual-mode resonator, two perturbing metal holes are set up on the diagonal of the lower dual-mode resonator cavity, which mainly affect the resonant frequency of the TE_{210} mode. The closer the two holes are, the higher the resonant frequency of the TE_{210} mode is, and the farther the holes are, the lower the resonant frequency of the TE_{210} mode is.

4. RESULTS AND ANALYSIS

4.1. Simulation Results of Filter A

To clarify the impact of changing the coupling slot length on the filter passband and FTZs, we maintain other parameters while altering the value of coupling slot length L_3 and observing the resulting change in the filter S-parameter curve. Figure 6 illustrates the outcomes of this experiment. The passband of the filter displays four distinct resonance points that align with the fourth-order coupling topology of the filter. There are two distinct FTZs located on either side of the passband. The existence of these FTZs is due to the equivalent negative coupling path of 1-3-4, as previously mentioned. As L_3 increases from 4 mm to 6 mm, the left edge of the filter passband migrates toward the lower frequencies; the right edge remains essentially unchanged; the positions of the FTZs move to the sides; and the passband of the filter is broadened.

The left-side position of the filter passband is primarily determined by the resonant frequency of the odd mode produced by the coupling of resonant cavities 1 and 3, namely TE_{110} and TE_{120} modes. The resonant frequency of these modes is impacted by the coupling coefficient M_{13}. A larger coupling coefficient leads to a lower resonant frequency. The resonant frequency of the even mode generated by the coupling of resonant cavities 1 and 2 (TE_{110} and TE_{210} modes) mainly determines the position of the right side of the passband of the filter. Its resonant frequency is nearly equal to the resonance frequency of the TE_{210} eigenmode. The change in the coupling coefficient M_{12} has a minor effect on its resonant frequency. When L_3 equals 6 mm, the transmission zero on the low-frequency side becomes indiscernible on the S_{21} curve. This occurs because the transmission zero is near the resonance frequency of the TE_{110} mode and is therefore overshadowed by the signal strength of that mode.

Similarly, in order to elucidate the impact of perturbation metal hole position variation in the dual-mode resonant cavity on filter passband and FTZs, other parameters were held constant while only the value of parameter c, determining the position of the perturbation metal hole, was altered to observe changes in filter S-parameter curves. The results obtained are depicted in Figure 7. It is evident that as c increases from 3.7 mm to 4.3 mm, the right side of the filter passband shifts towards higher frequencies while the left side remains essentially unchanged. Notably, when $c = 4.3$ mm, a distinct depression appears within the passband due to its pronounced influence on TE_{210} mode's electric field distribution and subsequent migration of its resonant frequency towards higher frequencies.

From the above analysis, it is evident that L_3 and c can be controlled to manipulate the passband and transmission zeros of the filter, resulting in improved filtering performance. After optimization, the center frequency of filter A is 4.72 GHz, with a 3 dB bandwidth of 0.14 GHz and a relative bandwidth of 3%. The rectangularity coefficient at 10 dB is approximately 1.2, while the return loss exceeds 15 dB. Additionally, the lower and upper rejection bands exhibit transmission zeros at frequencies of 4.35 GHz and 4.95 GHz, respectively. Furthermore, simulation results indicate a maximum insertion loss in the passband about 0.4 dB.

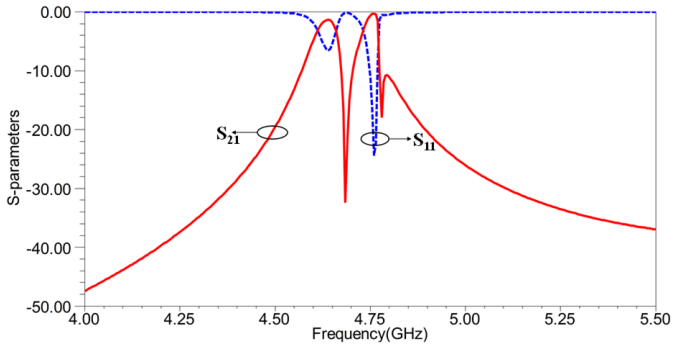

FIGURE 8. S-parameter curve of initial filter B.

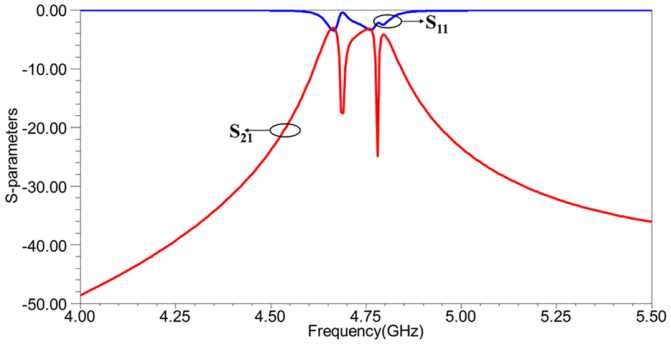

FIGURE 9. S-parameter curve for P_1 of 1.98 mm.

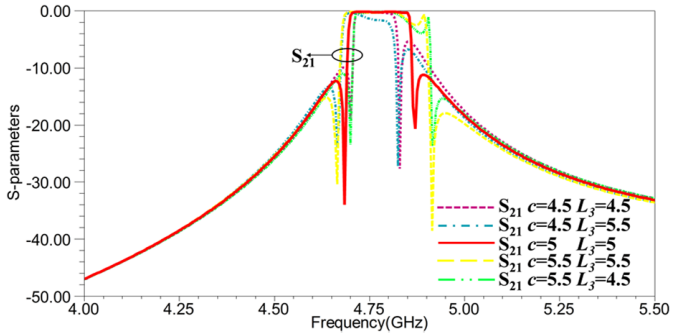

FIGURE 10. Parameter curves of filter S_{21} for different combinations of L_3 and c parameters.

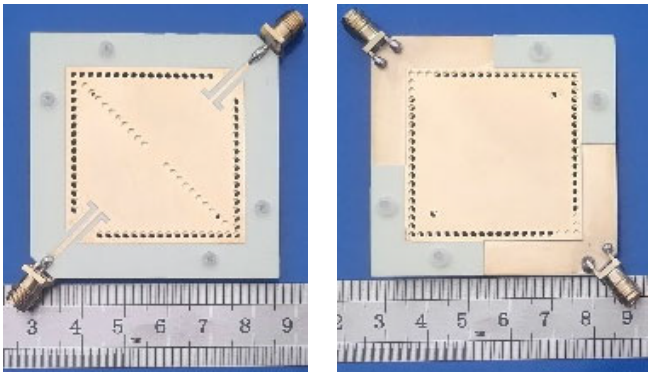

FIGURE 11. Filter object.

4.2. Simulation Results of Filter B

Based on the structure and dimensions of the optimized filter A, we added an inductive coupling window between the single-mode resonator cavities of the upper layer to form a 1–4 diagonal direct coupling path. The size of the coupling window is determined by L_5, initially set at 5 mm. The S-parameter curve of the filter is shown in Figure 8. The introduction of the 1–4 coupling path reduces the resonance frequency of the upper single-mode resonator to be lower than the resonance frequency of the lower dual-mode resonator's TE_{120} and TE_{210} modes, resulting in a change from one passband to two passbands. The passbands are formed by direct coupling of the two single-mode resonators on the upper layer, producing low-frequency passbands, and the lower dual-mode resonator, producing high-frequency passbands. The high-frequency passband retains two transmission zeros as a characteristic. To merge the two passbands into one, the upper single-mode resonator cavity can be reduced in size to match the dual-mode resonator's resonance frequency, for example, by setting P_1 to 1.98 mm. See Figure 9 for the filter S-parameter curve. At this time, the number of passbands of the filter is changed back to one, but the transmission zeros formed by the lower dual-mode resonator are located in the passband, resulting in an uneven and high-loss passband. Through the analysis of filter A, it is apparent that repositioning the transmission zeros towards the edge of the passband can be achieved by adjusting L_3 and c to meet the desired filtering characteristics. The curves depicting the parameters of filter S_{21} for various combinations of L_3 and c can be observed in Figure 10. It is evident from the figure that L_3 and c are efficient in controlling the passband and transmission zero positions of the filter. The dimensions of the final optimized filter B are shown in Table 2.

4.3. Comparison of Simulation and Test Results

Based on the dimensions outlined in Table 2, the printed circuit board (PCB) process was utilized to process physical filter B, which can be seen in Figure 11. The filter's physical size is $41 \times 41\ \text{mm}^2$ (exclusive of the input and output ports). To test the filter, it is necessary to solder SMA-KHD coaxial connectors to the input and output ports of the filter and connect them to an Agilent vector network analyzer (E8363C) for measurement. A depiction of the filter's S-parameter simulated and measured results can be observed in Figure 12. The overall trend of the measured and simulated S-parameter curves remains consistent, indicating a strong agreement between the two. The center frequency of the filter is observed to be 4.77 GHz, with a 3 dB bandwidth of 0.16 GHz and a relative bandwidth of 3.35%. Additionally, the rectangularity factor at 10 dB is approximately unity, while the return loss exceeds 15 dB. Notably, transmission zeros are found at frequencies of 4.68 GHz and 4.85 GHz for the lower and upper reject bands, respectively. Simulation results reveal an insertion loss in the passband around 0.35 dB; however, measurements indicate an increase of approximately 0.7 dB compared to simulation values. The disparity between measured and simulated values can

TABLE 3. Comparison with similar filters in the literature.

Refs.	f_0 (GHz)	FBW (%)	IL (dB)	Order	No. of TZs	Layer	size (λ_g^2)
[12]	5.2	3.31	1.62	4	1	1	0.96
[13]	15	4.3	1.7	4	2	1	1.64
[14]	10	3.28	1.15	4	2	2	0.74
[15]	5.5	3.6	1.2	4	0	2	0.77
[16]	30	4.03	2.74	4	4	1	\
[17]	10	3.3	1.55	4	2	1	2
This work	4.77	3.35	1.05	4	2	2	0.72

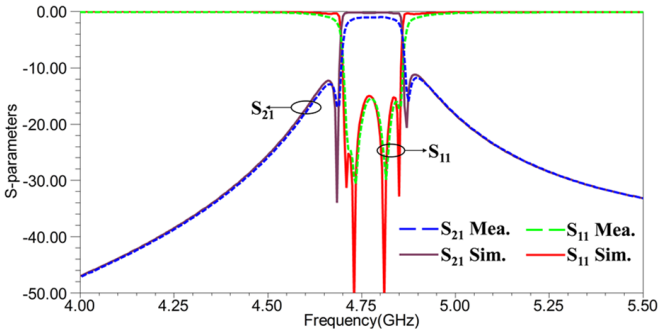

FIGURE 12. Simulated and measured filter S-parameters.

be primarily attributed to processing errors, dielectric losses, and conversion structure losses.

Table 3 provides a comparison of filter B proposed in this paper with the SIW filter cited in the references. The square-coupled topology filter, which consists of a combination of SIW dual-cavity single-mode and single-cavity dual-mode resonators proposed in this paper, has a compact size. It can effectively regulate the passbands and FTZ positions, thereby meeting the stopband requirements of various front-end RF systems. The FTZs can be achieved without the traditional negative coupling structure based on slot lines while still maintaining the higher Q-value advantage of SIW resonators. The approximate confinement of the space can also mitigate the effects of external environments on the filter's characteristics.

5. CONCLUSIONS

The equivalent coupling topologies of dual-cavity single-mode and single-cavity dual-mode resonator combination filters are analyzed in this paper. Two double-layer bandpass filters with different structures but equivalent square coupling topologies are proposed. The effects of the main parameters on the filter characteristics and transmission zero position are thoroughly analyzed. The second filter is fabricated and tested, showing simulation results that align well with the measured results. In this design, the flexibility and adjustability of passband and transmission zero points can be achieved by combining SIW dual-cavity single-mode and single-cavity dual-mode resonators, presenting a simple yet innovative design method. The rectangular coefficient of the filter closely approximates ideal values, rendering it applicable in the 5G (sub-6G) band.

ACKNOWLEDGEMENT

This work is supported by the Chongzuo Science and Technology Program Project (No. 2023ZC1112), the School-level Research Project of Guangxi Minzu Normal University (No. 2022SP007), and the Basic Research Ability Improvement Project for Young and Middle-Aged Teachers in Guangxi Universities (No. 2023KY0796).

REFERENCES

[1] Moscato, S., C. Tomassoni, M. Bozzi, and L. Perregrini, "Quarter-mode cavity filters in substrate integrated waveguide technology," *IEEE Transactions on Microwave Theory and Techniques*, Vol. 64, No. 8, 2538–2547, 2016.

[2] Jones, T. R. and M. Daneshmand, "Miniaturized folded ridged half-mode and quarter-mode substrate integrated waveguides for filter design," *IEEE Transactions on Microwave Theory and Techniques*, Vol. 67, No. 8, 3414–3426, 2019.

[3] Liu, Q., D. Zhang, M. Tang, H. Deng, and D. Zhou, "A class of box-like bandpass filters with wide stopband based on new dual-mode rectangular SIW cavities," *IEEE Transactions on Microwave Theory and Techniques*, Vol. 69, No. 1, 101–110, 2021.

[4] Li, P., H. Chu, and R.-S. Chen, "Design of compact bandpass filters using quarter-mode and eighth-mode SIW cavities," *IEEE Transactions on Components, Packaging and Manufacturing Technology*, Vol. 7, No. 6, 956–963, 2017.

[5] You, C. J., Z. N. Chen, X. W. Zhu, and K. Gong, "Single-layered SIW post-loaded electric coupling-enhanced structure and its filter applications," *IEEE Transactions on Microwave Theory and Techniques*, Vol. 61, No. 1, 125–130, 2013.

[6] Chen, X.-P. and K. Wu, "Substrate integrated waveguide cross-coupled filter with negative coupling structure," *IEEE Transactions on Microwave Theory and Techniques*, Vol. 56, No. 1, 142–149, 2008.

[7] Zhu, F., W. Hong, J.-X. Chen, and K. Wu, "Cross-coupled substrate integrated waveguide filters with improved stopband performance," *IEEE Microwave and Wireless Components Letters*, Vol. 22, No. 12, 633–635, 2012.

[8] Gong, K., W. Hong, Y. Zhang, P. Chen, and C. J. You, "Substrate integrated waveguide quasi-elliptic filters with controllable electric and magnetic mixed coupling," *IEEE Transactions on Microwave Theory and Techniques*, Vol. 60, No. 10, 3071–3078, 2012.

[9] Szydlowski, L., N. Leszczynska, and M. Mrozowski, "A linear phase filter in quadruplet topology with frequency-dependent couplings," *IEEE Microwave and Wireless Components Letters*, Vol. 24, No. 1, 32–34, 2014.

[10] Chu, P., W. Hong, M. Tuo, K.-L. Zheng, W.-W. Yang, F. Xu, and K. Wu, "In-line ports dual-mode substrate integrated waveguide filter with flexible responses," *IEEE Microwave and Wireless Components Letters*, Vol. 28, No. 10, 882–884, 2018.

[11] Li, M., Q. Ji, C. Chen, W. Chen, and H. Zhang, "A triple-mode bandpass filter with controllable bandwidth using QMSIW cavity," *IEEE Microwave and Wireless Components Letters*, Vol. 28, No. 8, 654–656, 2018.

[12] Liu, Q., D. Zhou, S. Wang, and Y. Zhang, "Highly-selective pseudoelliptic filters based on dual-mode substrate integrated waveguide resonators," *Electronics Letters*, Vol. 52, No. 14, 1233–1235, 2016.

[13] Chu, P., W. Hong, M. Tuo, K.-L. Zheng, W.-W. Yang, F. Xu, and K. Wu, "Dual-mode substrate integrated waveguide filter with flexible response," *IEEE Transactions on Microwave Theory and Techniques*, Vol. 65, No. 3, 824–830, 2017.

[14] Liu, Q., D. Zhou, D. Lv, D. Zhang, J. Zhang, and Y. Zhang, "Multi-layered dual-mode substrate integrated waveguide bandpass filter with input and output ports located on same substrate layer," *IET Microwaves, Antennas & Propagation*, Vol. 13, No. 15, 2641–2648, 2019.

[15] Lee, T.-H., W. Lin, and K. Wu, "Multilayer SIW dual-mode bandpass filter with higher-order mode attenuation," in *2018 IEEE MTT-S International Wireless Symposium (IWS)*, 1–3, Chengdu, China, 2018.

[16] Liu, Q., D.-F. Zhou, K. Gong, J.-H. Wang, D.-W. Zhang, and B.-H. Ma, "Dual- and triple-mode single-layer substrate-integrated waveguide filters based on higher-order modes for millimeter-wave applications," *IEEE Transactions on Circuits and Systems II: Express Briefs*, Vol. 71, No. 4, 1994–1998, Apr. 2024.

[17] Zhu, F., G. Q. Luo, B. You, X. H. Zhang, and K. Wu, "Planar dual-mode bandpass filters using perturbed substrate-integrated waveguide rectangular cavities," *IEEE Transactions on Microwave Theory and Techniques*, Vol. 69, No. 6, 3048–3057, Jun. 2021.